Supplementary information

Chirality manifestation in elastic coupling between the layers of double-walled carbon nanotubes

Sergei Rochal,[a,*] Dmitry Levshov,[a,b,†] Marina Avramenko,[a] Raul Arenal,[c,d] Thi Thanh Cao,[e] Van Chuc Nguyen,[e] Jean-Louis Sauvajol[b] and Matthieu Paillet[b]

[a]*Department of Nanotechnology, Faculty of Physics, Southern Federal University, 5, Zorge Street, Rostov-on-Don, 344090, Russia*

[b]*Laboratoire Charles Coulomb (UMR5221), CNRS-Université de Montpellier, Montpellier, F-34095, France*

[c]*Instituto de Nanociencia de Aragón, Campus Rìo Ebro, Edificio I+D. C/Mariano Esquillo, 50018, Zaragoza, Spain*

[d]*ARAID Foundation, 50018, Zaragoza, Spain*

[e]*Institute of Materials Science, Vietnam Academy of Science and Technology, 18 Hoang Quoc Viet, Hanoi, Vietnam*

[†]*present address: Physics Department, University of Antwerp, Universiteitsplein 1, B-2610 Antwerp, Belgium*

[*]E-mail: rochal_s@yahoo.fr

S1. Experimental data for structural characterization of individual DWCNTs. The index-assignments of individual DWCNTs, studied in this work, have been performed using the data presented in figures S1-S15. In the main text, see also Figure 1 and references to methods used for the structural characterization.

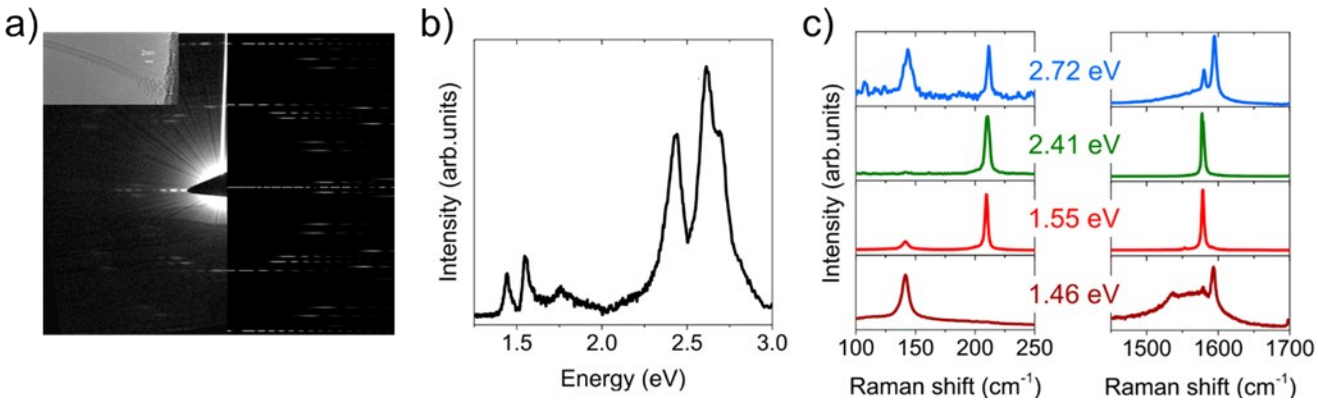

Figure S1. a) Experimental (left) and simulated (right) electron diffraction patterns, b) Rayleigh spectrum and c) RBLM (left) and G-band (right) ranges of Resonant Raman spectra of the individual DWCNT (14,1)@(15,12). Inset on panel a) shows the HRTEM image of this nanotube.

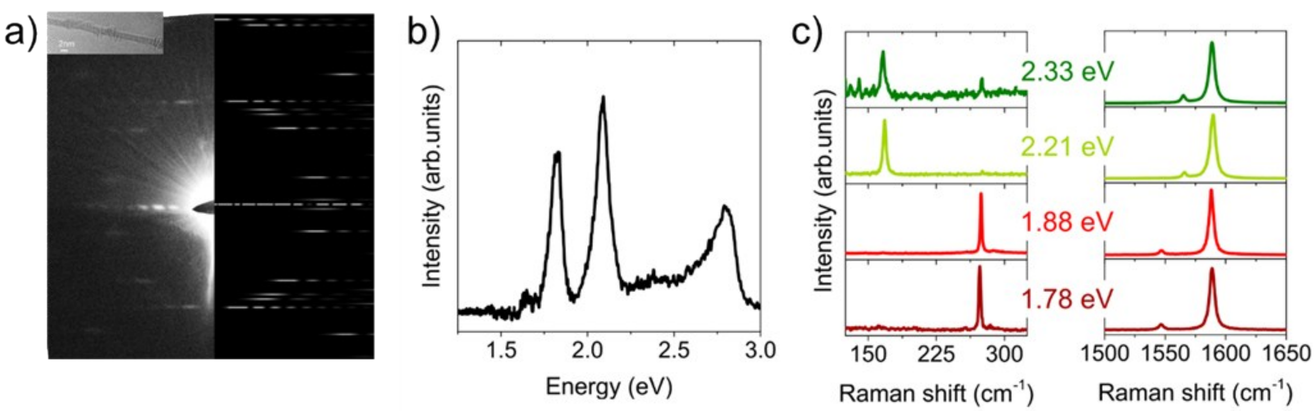

Figure S2. a) Experimental (left) and simulated (right) electron diffraction patterns, b) Rayleigh spectrum and c) RBLM (left) and G-band (right) ranges of Resonant Raman spectra of the individual DWCNT (7,6)@(16,6). Inset on panel a) shows the HRTEM image of this nanotube.

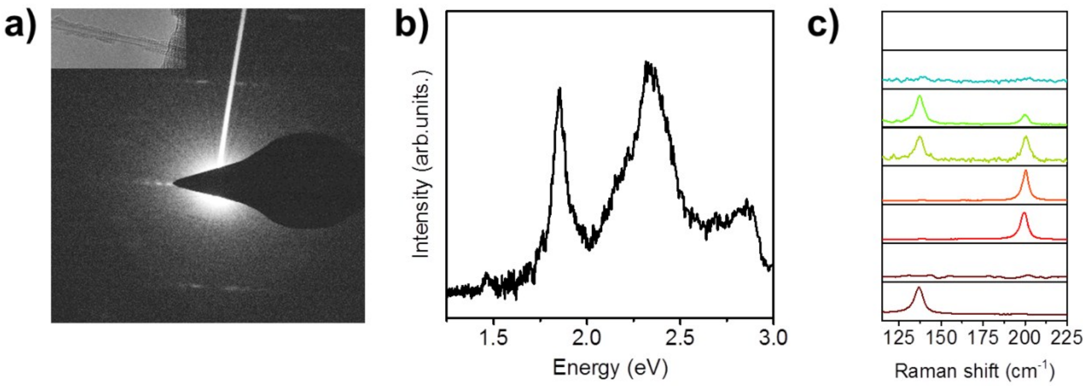

Figure S3. a) Experimental electron diffraction pattern, b) Rayleigh spectrum and c) RBLM (left) and G-band (right) ranges of Resonant Raman spectra of the individual DWCNT (14,2)@(22,4). Inset on panel a) shows the HRTEM image of this nanotube.

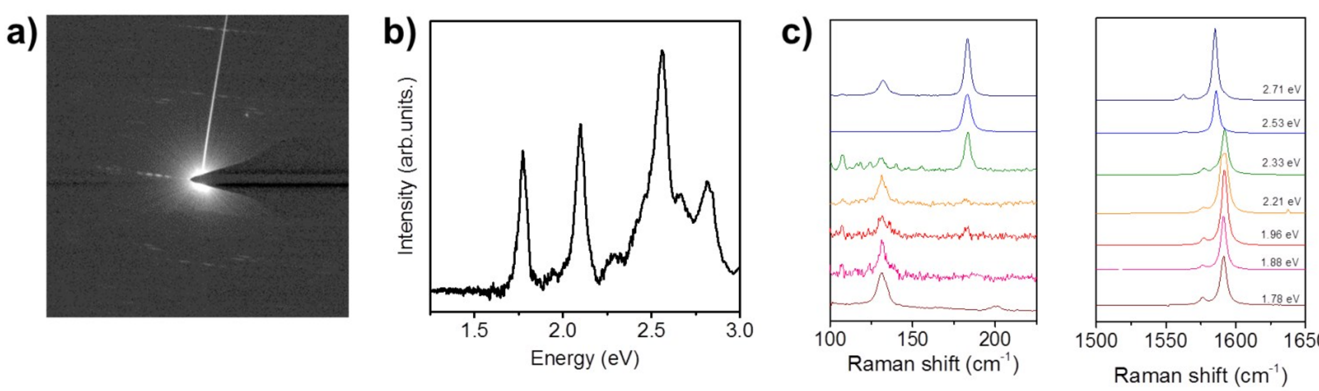

Figure S4. a) Experimental electron diffraction pattern, b) Rayleigh spectrum and c) RBLM (left) and G-band (right) ranges of Resonant Raman spectra of the individual DWCNT (16,2)@(16,14).

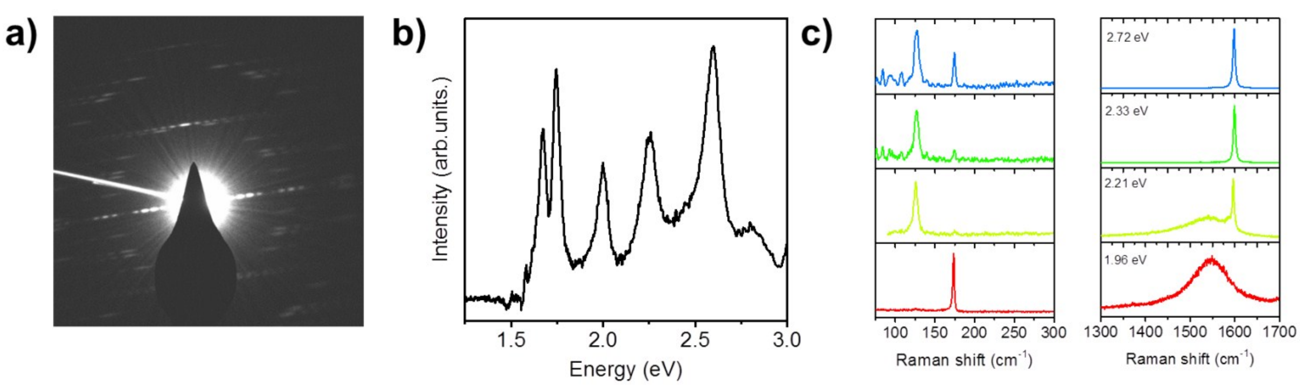

Figure S5. a) Experimental electron diffraction pattern, b) Rayleigh spectrum and c) RBLM (left) and G-band (right) ranges of Resonant Raman spectra of the individual DWCNT (14,5)@(26,1).

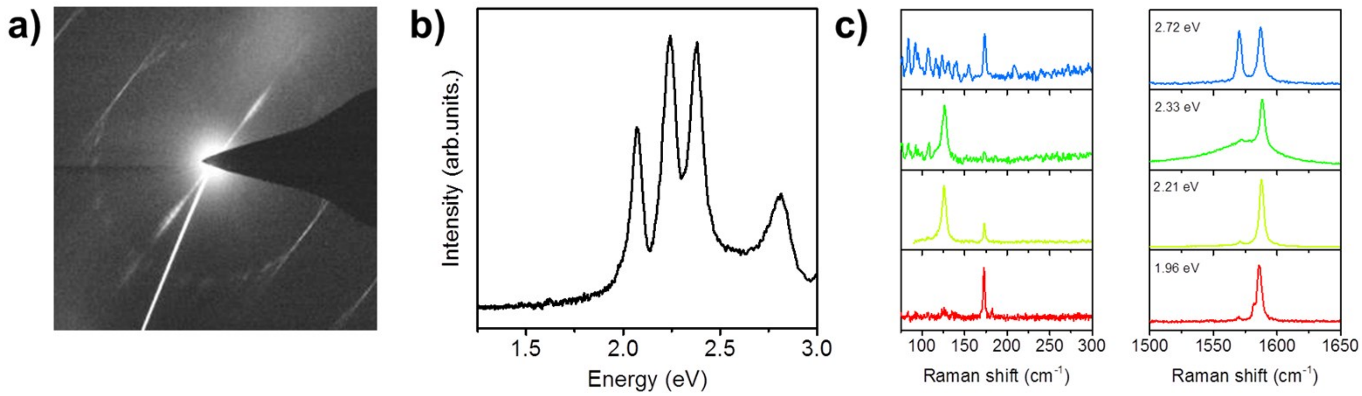

Figure S6. a) Experimental electron diffraction pattern, b) Rayleigh spectrum and c) RBLM (left) and G-band (right) ranges of Resonant Raman spectra of the individual DWCNT (18,2)@(19,13).

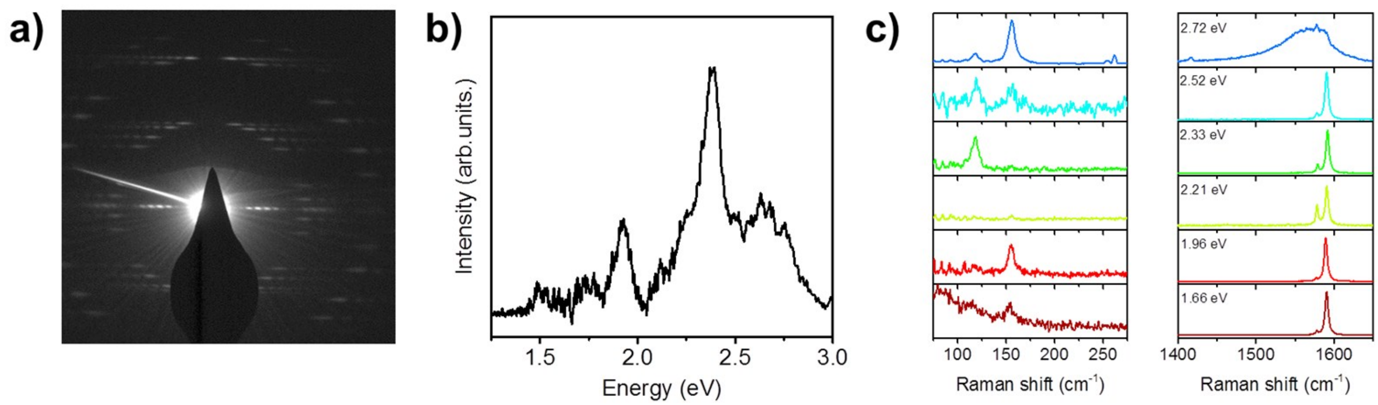

Figure S7. a) Experimental electron diffraction pattern, b) Rayleigh spectrum and c) RBLM (left) and G-band (right) ranges of Resonant Raman spectra of the individual DWCNT (18,6)@(21,14).

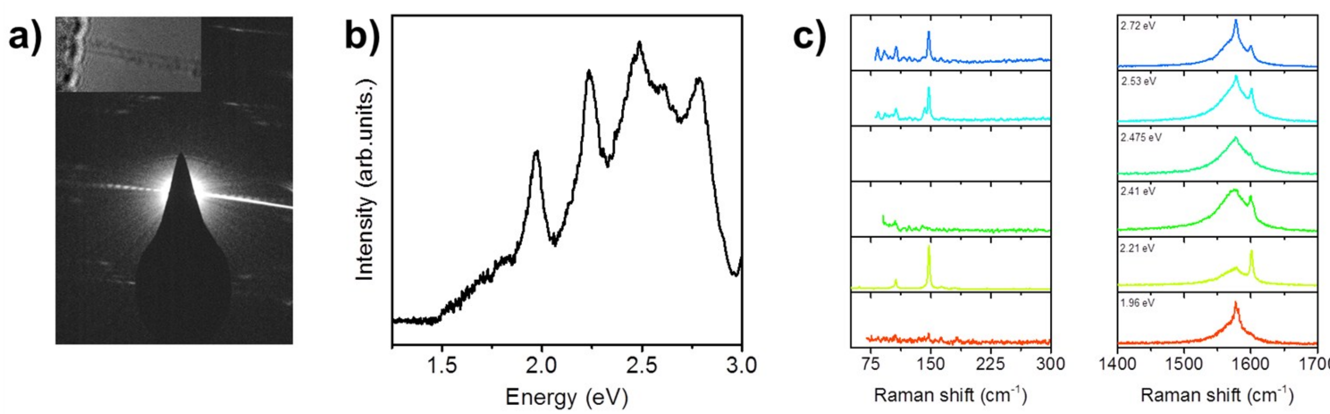

Figure S8. a) Experimental electron diffraction pattern, b) Rayleigh spectrum and c) RBLM (left) and G-band (right) ranges of Resonant Raman spectra of the individual DWCNT (17,14)@(26,14). Inset on panel a) shows the HRTEM image of this nanotube.

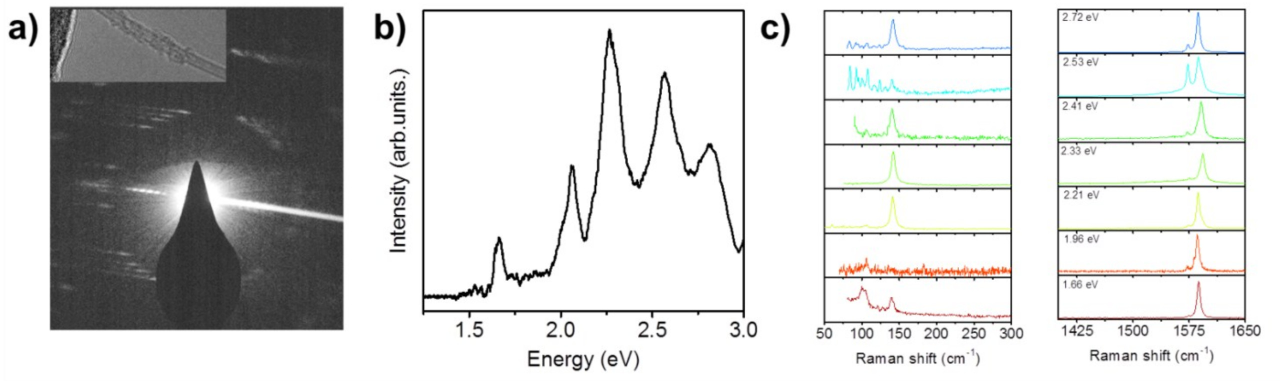

Figure S9. a) Experimental electron diffraction pattern, b) Rayleigh spectrum and c) RBLM (left) and G-band (right) ranges of Resonant Raman spectra of the individual DWCNT (17,14)@(28,12). Inset on panel a) shows the HRTEM image of this nanotube.

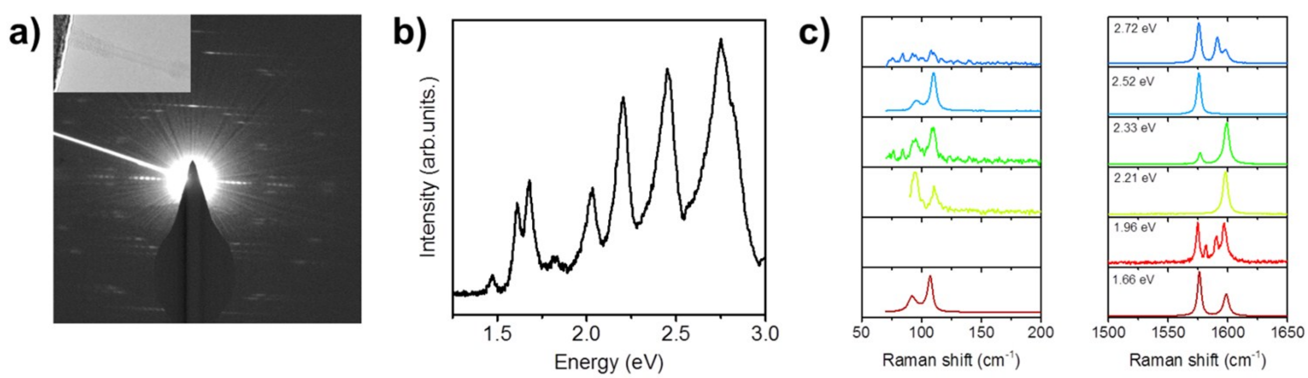

Figure S10. a) Experimental electron diffraction pattern, b) Rayleigh spectrum and c) RBLM (left) and G-band (right) ranges of Resonant Raman spectra of the individual DWCNT (30,1)@(27,19). Inset on panel a) shows the HRTEM image of this nanotube.

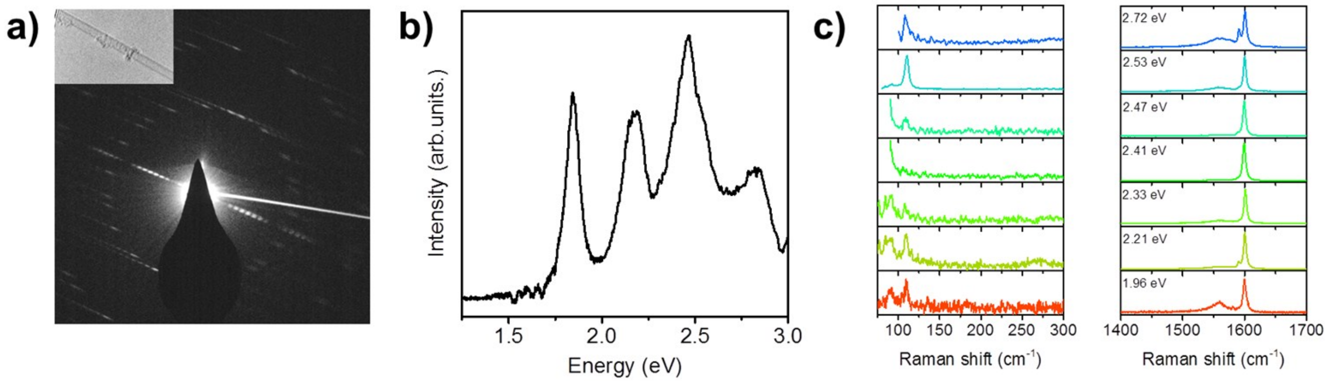

Figure S11. a) Experimental electron diffraction pattern, b) Rayleigh spectrum and c) RBLM (left) and G-band (right) ranges of Resonant Raman spectra of the individual DWCNT (22,13)@(39,2). Inset on panel a) shows the HRTEM image of this nanotube.

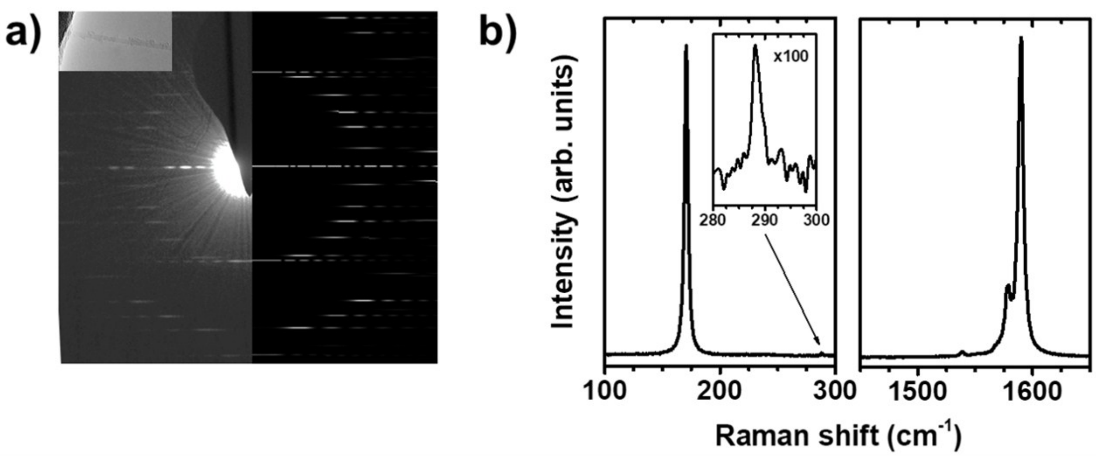

Figure S12. a) Experimental (left) and simulated (right) electron diffraction patterns and b) RBLM (left) and G-band (right) ranges of Resonant Raman spectra of the individual DWCNT (8,4)@(18,2). Inset on panel a) shows the HRTEM image of this nanotube.

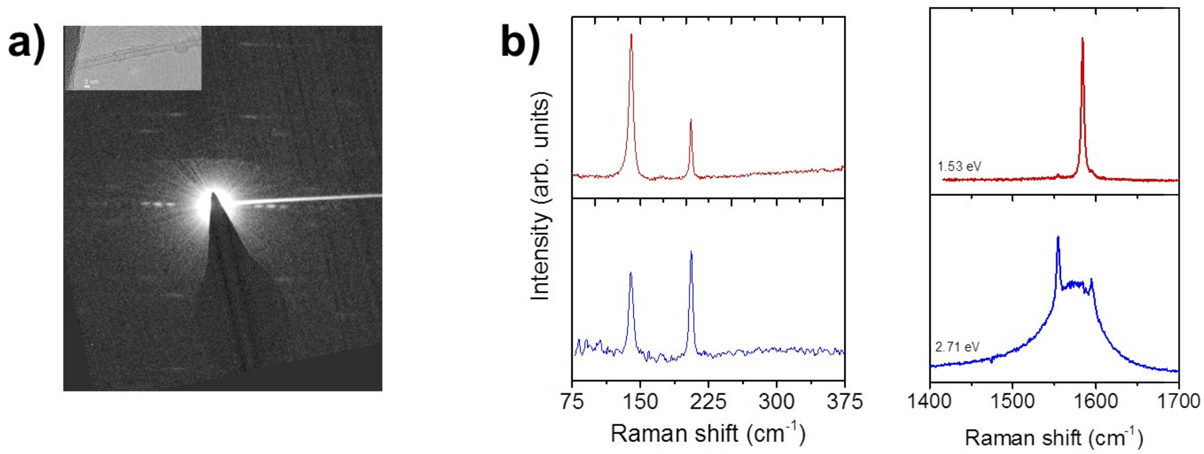

Figure S13. a) Experimental electron diffraction pattern and b) RBLM (left) and G-band (right) ranges of Resonant Raman spectra of the individual DWCNT (11,6)@(18,9). Inset on panel a) shows the HRTEM image of this nanotube.

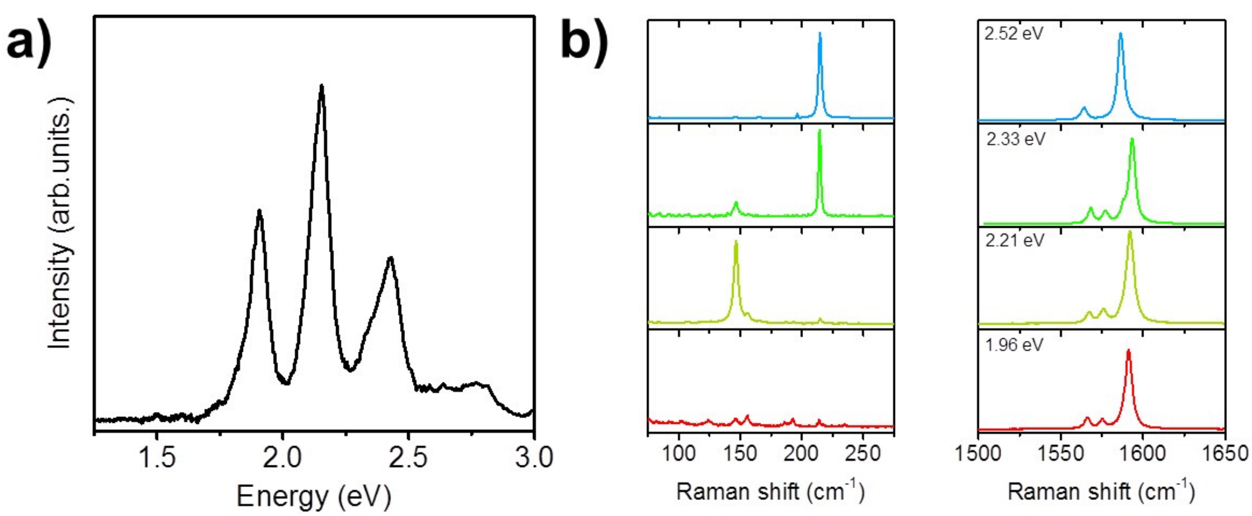

Figure S14. a) Rayleigh spectrum and b) RBLM (left) and G-band (right) ranges of Resonant Raman spectra of the individual DWCNT (14,1)@(21,4).

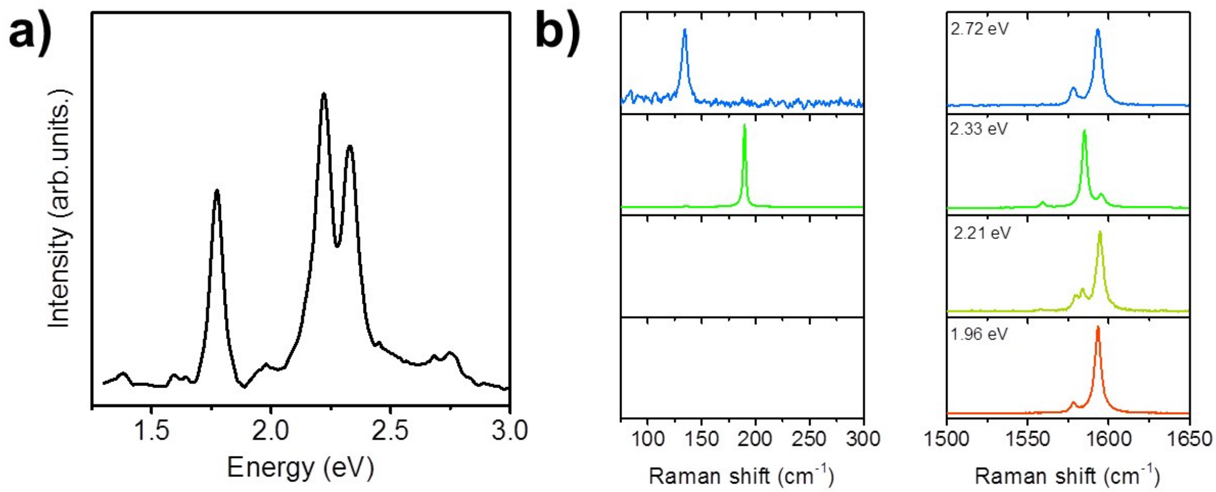

Figure S15. a) Rayleigh spectrum and b) RBLM (left) and G-band (right) ranges of Resonant Raman spectra of the individual DWCNT (15,2)@(23,4).

S2. Some statistical information on DWCNTs. Let us consider the abundance of DWCNTs as a function of $|\theta_{in}| - |\theta_{out}|$. In the range between minimal inner and maximal outer diameters, namely 0.6…6.6 nm, N = 125558 DWCNTs are theoretically possible provided that the interlayer distance is from 0.3001 to 0.4012 nm. In the histogram S16 the height of the blue bars is defined as $\Delta N/N$, where ΔN represents the number of theoretically possible DWCNTs, which belong to the angular interval of 0.85° equal to the angular width of the bars. Such form of theoretical probability density distribution as a function of $|\theta_{in}| - |\theta_{out}|$ is explained by the fact that theoretically possible DWCNTs are distributed almost uniformly in variables $|\theta_{in}|$ and $|\theta_{out}|$. In order to obtain analogous brown histogram, 335 DWCNTs were taken from the papers[S1–S11,S13-S18] and analyzed.

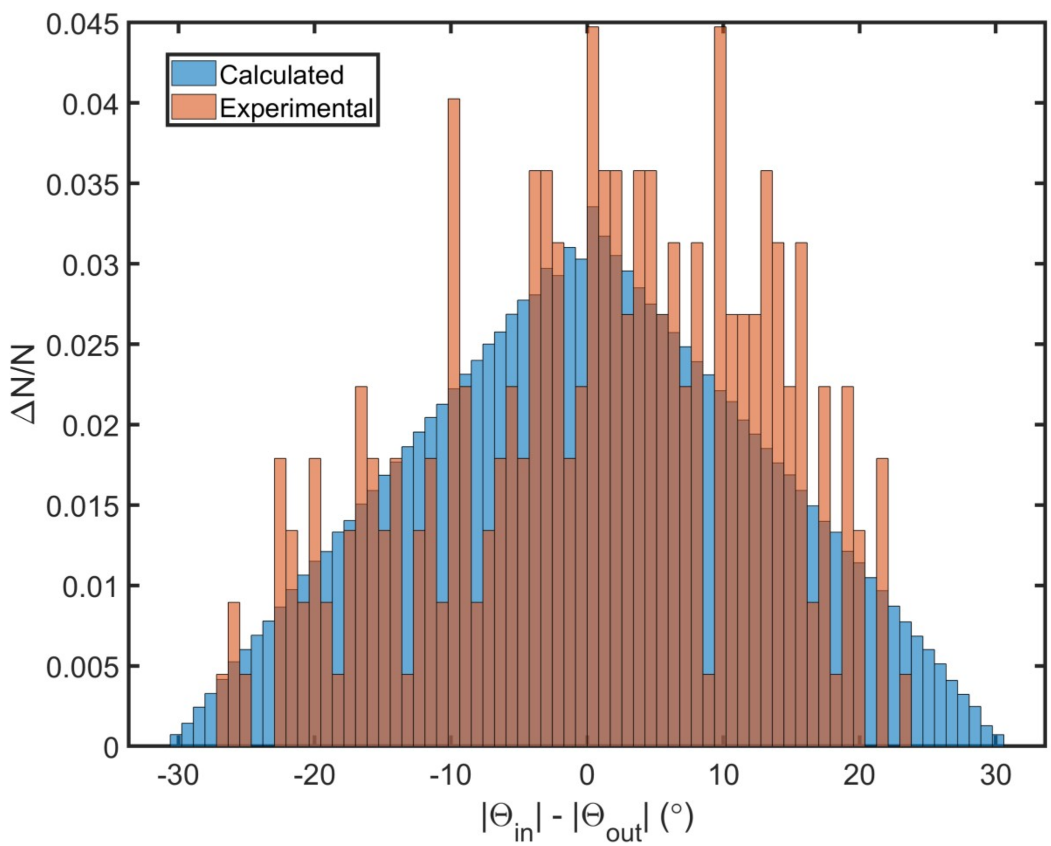

Figure S16. Theoretical and experimental probability density distribution of DWCNTs. Our recent results are added to the known data on DWCNTs taken from the Refs. S1–S11,S13-S18. The data presented in Ref. S12 are not included, because the values $|\theta_{in}| - |\theta_{out}|$ cannot be explicitly determined from that paper.

S3. Structural information for individual DWCNTs and their measured and calculated frequencies of radial breathing-like modes

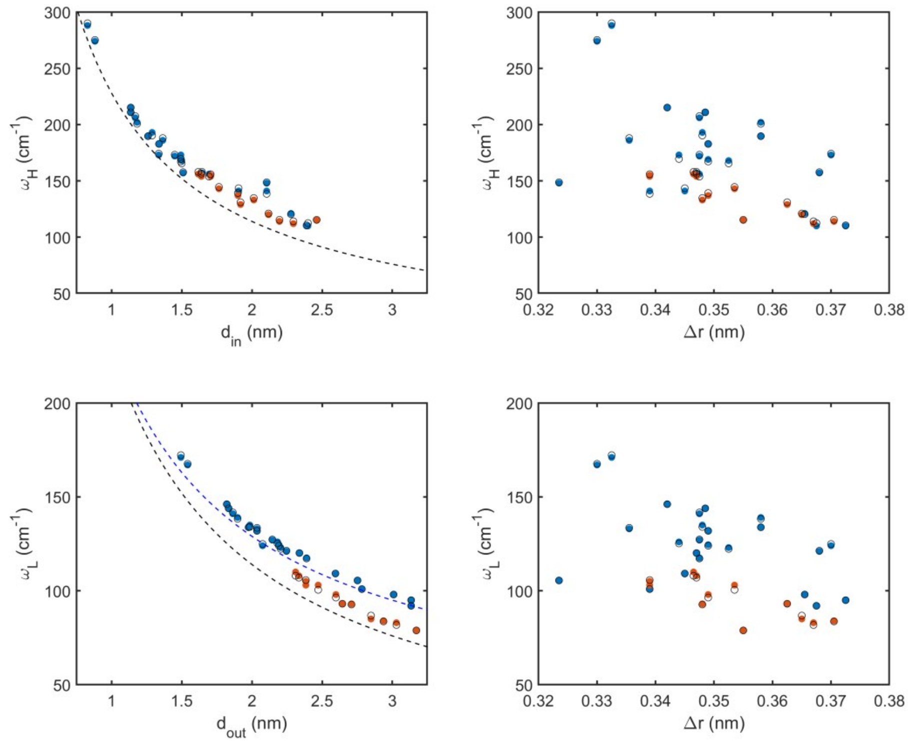

Figure S18. Experimental results and their modeling. The filled blue circles correspond to the experimental data of the in-phase (ω_L) and out-of-phase (ω_H) RBLMs of the 24 DWCNTs studied in this work (Table 1), while the red ones represent the analogous data from Ref. S2. The calculations within the framework of our model (Eq. 4) by using parameters (7) for the DWCNTs studied in the present work and parameters (8) for those of Ref. S2 are shown with unfilled circles. In the first column, the dotted black and blue lines represent the diameter dependence of the RBM frequency in SWCNTs calculated by using Eq. (5) with $C' = 0$ nm^{-2} and $C' = 3380$ nm^{-2}, respectively. One can see that the dispersions for the in-phase (ω_L) and out-of-phase (ω_H) RBLMs are substantially different from the ones for RBMs of constituent SWCNTs. At first sight, no correlation can be found between the data plotted in the third column (corresponding to the dependence of the RBLM frequencies on the twist angle). Nevertheless, this correlation is determined with a good degree of accuracy within the framework of the proposed model. The divergence between theoretical and experimental RBLM frequencies for the majority of plotted points is less than the circle size.

S4. An example of structural identification of three DWCNTs. We have got three individual DWCNTs, whose structures haven't been unambiguously identified within the existing approaches. Table S1 includes 7 rows that correspond to the alternative variants of structural identification of these DWCNTs. The first and the second DWCNTs could be identified in two ways, the latter one – in three.

Table S1. The alternative variants of structural identification of three DWCNTs.

1	2	3	4	5	6	7	8	9	10	11	12	13	14
№	(n_i, m_i)	(n_o, m_o)	d_{in}	d_{out}	$\lvert\Delta\theta\rvert$	ω^{exp}_{L}	ω^{exp}_{H}	C'	G'	G'_{fit}	ω^{theor}_{L}	ω^{theor}_{H}	$\Delta\omega$
1	(10, 6)	(14, 13)	1.096	1.831	6.99	140	212	3193.6	880.5	640.6	139.1	210.9	0.98
1	(10, 6)	(16, 11)	1.096	1.841	2.11	140	212	3366.3	880.6	224.8	137.6	209	2.68
2	(13, 5)	(18, 11)	1.260	1.985	6.46	133	188	3185.6	1507	1396.8	132.7	187.5	0.44
2	(13, 5)	(22, 6)	1.260	1.999	3.87	133	188	3378.4	1507.8	791.1	130.8	184.5	2.88
3	(21, 17)	(30, 19)	2.581	3.350	3.9	86	102	2513.3	2078.1	1891.6	86	100.8	0.88
3	(22, 17)	(30, 20)	2.651	3.413	2.36	86	102	2932.6	2243.9	2351.2	86	102.7	0.49
3	(24, 16)	(29, 22)	2.730	3.469	2.06	86	102	3519.0	2281.0	3537.2	86.1	109.6	5.4

The first eight columns of this Table contain structural data and RBLM frequencies. The values of C' and G' are calculated for each of the 7 variants and presented in columns 9 and 10. In order to determine them, two Eqs. (4) are simultaneously solved for each nanotube: in the first copy of Eq. (4) both terms ω^2 are substituted with squared ω^{exp}_{H} , in the latter one – with squared ω^{exp}_{L}, where ω^{exp}_{L} and ω^{exp}_{H} are the lower (in-phase) and higher (out-of-phase) experimentally observed RBLM frequencies, respectively (see columns 7 and 8). Then the system obtained is solved in G' and C' variables (see the description of these values and the discussion of this solution in the main text). The next column entitled G'_{fit} presents G' obtained by means of Eq. (6) with coefficients (7). The comparison of columns 10 and 11 establishes that the first, the third and the sixth rows of the Table S1 are the best ones to match, respectively, the first, second and third DWCNTs considered, i.e. where the coefficients G' and G'_{fit} have the closest values.

We have also calculated, by using Eq. 4, the theoretical RBLM frequencies ω^{theor}_{H} and ω^{theor}_{L} for each of the 7 variants (see columns 12 and 13). The last column contains deviations $\Delta\omega = \sqrt{((\omega^{theor}_{L} - \omega^{exp}_{L})^2 + (\omega^{theor}_{H} - \omega^{exp}_{H})^2)/2}$ of theoretical frequencies from the experimental ones. The smallest $\Delta\omega$ values are found for the same DWCNT indexations as using the former G' and G'_{fit}

comparison. For the third DWCNT, the overall better agreement using both criteria (closest $G^{'}$ and $G_{fit}^{'}$ values and smallest $\Delta\omega$ values) favors the (21,18)@(30,20). However, the agreement is rather good also for the (21,17)@(30,19), which cannot be fully excluded.

Below we present a very simple program prepared in Maple computing environment. It has been used in order to obtain the values presented in columns 9-14 of Table S1. Thus, the identification of the structures of three considered DWCNTs has been performed.

restart:
#input data
$\Delta\theta$:=*array*(1..7,[6.99, 2.11, 6.46, 3.87, 3.9, 2.36, 2.06]):
d_i:=*array*(1..7,[1.096, 1.096, 1.260, 1.260, 2.581, 2.651, 2.730]): *#inner diameters*
d_o:=*array*(1..7,[1.831, 1.841, 1.985, 1.999, 3.350, 3.413, 3.469]): *#outer diameters*
ω_L:=*array*(1..7,[140, 140, 133, 133, 86, 86, 86]): *#experimental frequencies*
ω_H:=*array*(1..7,[212, 212, 188, 188, 102, 102, 102]): *#experimental frequencies*
G_0:=31644: G_1:= − 45839: G_2:=882: G_3:=49:

#C_prime=C', G_prime=G'
for j **from** 1 **to** 7 **do**

$$eq1:=simplify\left(\left(\frac{d_o[j]}{2}\cdot\left(\left(\frac{228}{d_o[j]}\right)^2+C\_prime-(\omega_L[j])^2\right)+G\_prime\right)\cdot\left(\frac{d_i[j]}{2}\cdot\left(\left(\frac{228}{d_i[j]}\right)^2-(\omega_L[j])^2\right)+G\_prime\right)-(G\_prime)^2\right):$$

$$eq2:=simplify\left(\left(\frac{d_o[j]}{2}\cdot\left(\left(\frac{228}{d_o[j]}\right)^2+C\_prime-(\omega_H[j])^2\right)+G\_prime\right)\cdot\left(\frac{d_i[j]}{2}\cdot\left(\left(\frac{228}{d_i[j]}\right)^2-(\omega_H[j])^2\right)+G\_prime\right)-(G\_prime)^2\right):$$

sol[*j*]:=*fsolve*({*eq1*,*eq2*},{*C_prime* = 1,*G_prime* = 3000}):
G_prime[*j*]:=*solve*(*sol*[*j*][2]):
C_prime[*j*]:=*solve*(*sol*[*j*][1]):
end do;

#$G\_prime\_fit = G_{fit}^{'}$
for j **from** 1 **to** 7 **do**

$$G\_prime\_fit[j]:=evafl\left(G_0+G_1\cdot(d_o[j]-d_i[j])+G_2\cdot(d_o[j]+d_i[j])+G_3\cdot(d_o[j]+d_i[j])\cdot\cos\left(\frac{6\cdot\Delta\theta[j]\cdot\pi}{180}\right)\right):$$

$$eq3:=simplify\left(\left(\frac{d_o[j]}{2}\cdot\left(\left(\frac{228}{d_o[j]}\right)^2+C\_prime[j]-w\right)+G\_prime\_fit[j]\right)\cdot\left(\frac{d_i[j]}{2}\cdot\left(\left(\frac{228}{d_i[j]}\right)^2-w\right)+G\_prime\_fit[j]\right)-(G\_prime\_fit[j])^2\right):$$

sol:=*fsolve*(*eq3*,*w*):
*theor_*ω_L[*j*]:=*sqrt*(*sol*[1]):
*theor_*ω_H[*j*]:=*sqrt*(*sol*[2]):

$$\Delta\omega[j]:=\sqrt{\frac{\left((theor\_\omega_L[j]-\omega_L[j])^2+(theor\_\omega_H[j]-\omega_H[j])^2\right)}{2}}:$$

end do;

REFERENCES

(S1) Liu, K.; Jin, C.; Hong, X.; Kim, J.; Zettl, A.; Wang, E.; Wang, F. Van Der Waals-Coupled Electronic States in Incommensurate Double-Walled Carbon Nanotubes. *Nat. Phys.* 2014, *10*, 737–742.

(S2) Liu, K.; Hong, X.; Wu, M.; Xiao, F.; Wang, W.; Bai, X.; Ager, J. W.; Aloni, S.; Zettl, A.; Wang, E.; *et al.* Quantum-Coupled Radial-Breathing Oscillations in Double-Walled Carbon Nanotubes. *Nat. Commun.* 2013, *4*, 1375.

(S3) Zuo, J.-M.; Kim, T.; Celik-Aktas, A.; Tao, J. Quantitative Structural Analysis of Individual Nanotubes by Electron Diffraction. *Zeitschrift für Krist.* 2007, *222*, 625–633.

(S4) Gao, M.; Zuo, J. M.; Zhang, R.; Nagahara, L. A. Structure Determinations of Double-Wall Carbon Nanotubes Grown by Catalytic Chemical Vapor Deposition. *J. Mater. Sci.* 2006, *41*, 4382–4388.

(S5) Colomer, J.-F.; Henrard, L.; Launois, P.; Van Tendeloo, G.; Lucas, A. A.; Lambin, P. Bundles of Identical Double-Walled Carbon Nanotubes. *Chem. Commun.* 2004, *0*, 2592.

(S6) Liu, K.; Xu, Z.; Wang, W.; Gao, P.; Fu, W.; Bai, X.; Wang, E. Direct Determination of Atomic Structure of Large-Indexed Carbon Nanotubes by Electron Diffraction: Application to Double-Walled Nanotubes. *J. Phys. D. Appl. Phys.* 2009, *42*, 125412.

(S7) Colomer, J.-F.; Henrard, L.; Launois, P.; Van Tendeloo, G.; Lucas, A. A.; Lambin, P. Interpretation of Electron Diffraction from Carbon Nanotube Bundles Presenting Precise Helicity. *Phys. Rev. B* 2004, *70*, 075408.

(S8) Zhu, H.; Suenaga, K.; Hashimoto, A.; Urita, K.; Iijima, S. Structural Identification of Single and Double-Walled Carbon Nanotubes by High-Resolution Transmission Electron Microscopy. *Chem. Phys. Lett.* 2005, *412*, 116–120.

(S9) Zhu, H.; Suenaga, K.; Wei, J.; Wang, K.; Wu, D. Atom-Resolved Imaging of Carbon Hexagons of Carbon Nanotubes. *J. Phys. Chem. C* 2008, *112*, 11098–11101.

(S10) Guan, L.; Suenaga, K.; Iijima, S. Smallest Carbon Nanotube Assigned with Atomic Resolution Accuracy. *Nano Lett.* 2008, *8*, 459–462.

(S11) Qin, L.-C. Determination of the Chiral Indices (n,m) of Carbon Nanotubes by Electron Diffraction. *Phys. Chem. Chem. Phys.* 2007, *9*, 31–48.

(S12) Ghedjatti, A.; Magnin, Y.; Fossard, F.; Wang, G.; Amara, H.; Flahaut, E.; Lauret, J.-S.; Loiseau, A. Structural Properties of Double-Walled Carbon Nanotubes Driven by Mechanical Interlayer Coupling. *ACS Nano* 2017, *11*, 4840–4847.

(S13) Hashimoto, A.; Suenaga, K.; Urita, K.; Shimada, T.; Sugai, T.; Bandow, S.; Shinohara, H.; Iijima, S. Atomic Correlation between Adjacent Graphene Layers in Double-Wall Carbon Nanotubes. *Phys. Rev. Lett.* 2005, *94*, 1–4.

(S14) Hirahara, K.; Kociak, M.; Bandow, S.; Nakahira, T.; Itoh, K.; Saito, Y.; Iijima, S. Chirality Correlation in Double-Wall Carbon Nanotubes as Studied by Electron Diffraction. *Phys. Rev. B* 2006, *73*, 195420.

(S15) Zhao, S.; Kitagawa, T.; Miyauchi, Y.; Matsuda, K.; Shinohara, H.; Kitaura, R. Rayleigh Scattering Studies on Inter-Layer Interactions in Structure-Defined Individual Double-Wall Carbon Nanotubes. *Nano Res.* 2014, *7*, 1548–1555.

(S16) Kociak, M.; Suenaga, K.; Hirahara, K.; Saito, Y.; Nakahira, T.; Iijima, S. Linking Chiral Indices and Transport Properties of Double-Walled Carbon Nanotubes. *Phys. Rev. Lett.* 2002, *89*, 155501.

(S17) Kociak, M.; Hirahara, K.; Suenaga, K.; Iijima, S. How Accurate Can the Determination of Chiral Indices of Carbon Nanotubes Be? *Eur. Phys. J. B - Condens. Matter* 2003, *32*, 457–469.

(S18) Zuo, J. M. M. Atomic Resolution Imaging of a Carbon Nanotube from Diffraction Intensities. *Science* 2003, *300*, 1419–1421.